

PURE: Turning Polysemantic Neurons Into Pure Features by Identifying Relevant Circuits

Maximilian Dreyer¹, Erblina Puelku¹, Johanna Vielhaben¹,
Wojciech Samek^{1,2,3,†}, Sebastian Lapuschkin^{1,†}

¹ Fraunhofer Heinrich Hertz Institute, ² Technical University of Berlin,

³ BIFOLD – Berlin Institute for the Foundations of Learning and Data

[†]corresponding authors: {wojciech.samek | sebastian.lapuschkin}@hhi.fraunhofer.de

Abstract

The field of mechanistic interpretability aims to study the role of individual neurons in Deep Neural Networks. Single neurons, however, have the capability to act polysemantically and encode for multiple (unrelated) features, which renders their interpretation difficult. We present a method for disentangling polysemanticity of any Deep Neural Network by decomposing a polysemantic neuron into multiple monosemantic “virtual” neurons. This is achieved by identifying the relevant sub-graph (“circuit”) for each “pure” feature. We demonstrate how our approach allows us to find and disentangle various polysemantic units of ResNet models trained on ImageNet. While evaluating feature visualizations using CLIP, our method effectively disentangles representations, improving upon methods based on neuron activations. Our code is available at <https://github.com/maxdreyer/PURE>.

1. Introduction

The field of eXplainable Artificial Intelligence (XAI) aims to increase the transparency of Deep Neural Networks (DNNs). Several XAI works study the role of a model’s latent neurons and their interactions [18, 19], which recently developed into the sub-field of *mechanistic interpretability*. Neurons are commonly viewed as feature extractors corresponding to human-interpretable concepts [1, 3, 18]. However, neurons can be *polysemantic*, meaning that they extract multiple (unrelated) features, which adds ambiguity to their interpretability. Other XAI works study *circuits*, i.e., distinct sub-graphs of a network performing specific sub-tasks, which recently became popular for Large Language Models (LLMs) [9, 11, 28]. Notably, the interpretability of a circuit depends on the interpretability of its units, which again can be polysemantic. In applications, such as knowledge discovery or validation of DNNs in safety-

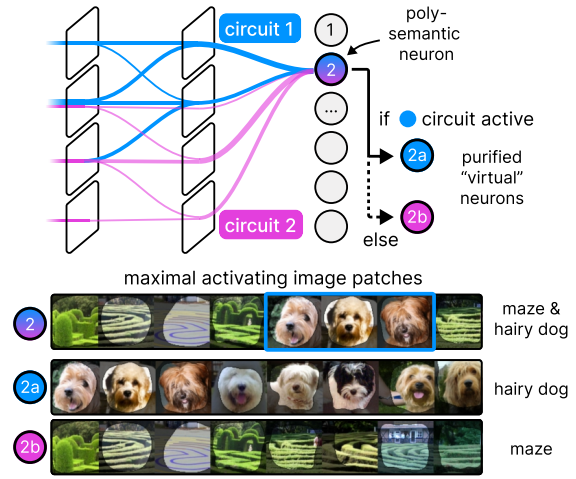


Figure 1. Distinct circuits exist for each feature of a polysemantic neuron. With PURE, we propose to split a polysemantic neuron into multiple pure “virtual” ones, one for each circuit. Here, we disentangle the maximally activating sample (patches) of neuron 2 into its two pure features: “hairy dog” (2a) and “maze” (2b).

critical tasks, high latent interpretability is crucial for XAI usefulness [4, 8]. In this work, we build on the assumption that for each monosemantic (“pure”) feature a unique sub-graph exists. Identifying the active circuits then allows disentangling a polysemantic unit into multiple “virtual” pure units (with one circuit each), as shown in Fig. 1 where we disentangle a neuron encoding for dog and maze features.

To that end, we introduce Purifying Representations (PURE), a post-hoc approach for increasing interpretability of latent representations by disentangling polysemantic neurons into pure features. PURE is based on discovering the relevant (active) circuit of each semantics, which is identified via a partial backward pass. Through the means of foundational models, we measure a significant increase in interpretability of ResNet [12] models after applying PURE, also improving upon activation-based approaches.

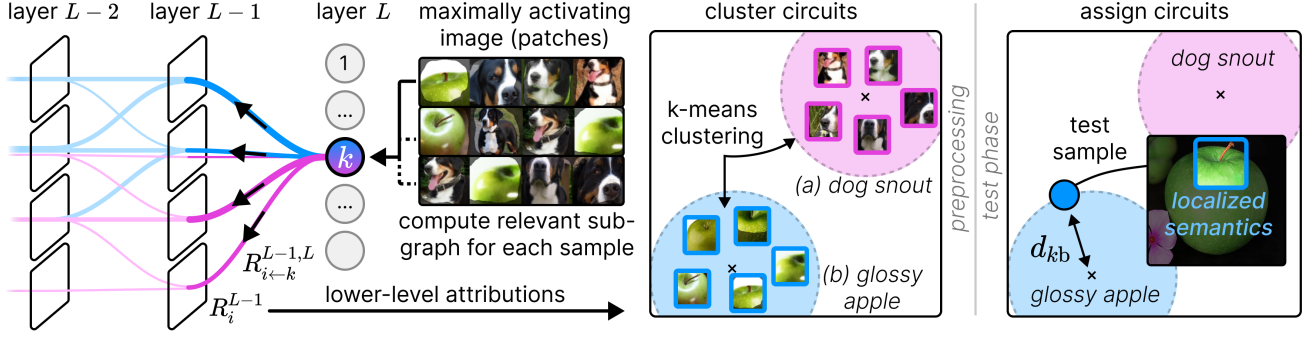


Figure 2. PURE detects circuits using lower-level neuron attributions for the n_{ref} most activating input samples in a preprocessing step. For polysemantic neurons, we assume distinct active circuits for each semantics, which are found through clustering attributions with k -means. During test phase, the active circuit can be assigned post-hoc for any new test sample by identifying the closest circuit.

2. Related Work

Various works have shown that neurons in DNNs encode for distinct features that can often be interpreted by humans [1, 3, 5]. However, besides redundancies in representations, an occurring problem is the polysemanticity of neurons. As such, interpretation of the latent space is difficult. For concept-based explanations, feature visualizations are confusing, or ambiguous as it might be unclear, which semantics are actually present. Further, semantics can be overlooked, *e.g.*, when one feature is more dominant than another [17]. As a way out, some works propose to find more meaningful directions [10, 14] or subspaces in latent space [27], but they often require pre-defined concepts or reconstruct the latent space only partially. To resolve poly-semanticity on a neuron level, O’Mahony *et al.* [20] propose to find directions (*i.e.*, a linear combination of neurons) based on latent activations. Instead of activations (that depend on *all* present input features), PURE is based on neuron-specific circuits which is more specific to the role of a neuron and leads to an improved disentanglement.

Circuits, in general, are viewed as the sub-graphs of a neural network architecture [28] that perform a specific task. They further consist of a set of linked features and the weights between them [19]. In recent work, circuit analysis [24] has been extended beyond convolution-based architectures [6] to, *e.g.*, transformer-based models [9, 11, 28]. The discovery of circuits has been partially automatized both for computer vision [23] and language models [7].

3. Method

For PURE, we view circuits as directed acyclic graphs that consist of nodes R_j^l for neuron j in layer l and edges $R_{i \leftarrow j}^{l-1,l}$ connecting nodes j and i of adjacent layers. We hypothesize that polysemanticity of a neuron arises because multiple circuits share one node, as illustrated in Fig. 2. PURE disentangles these circuits from a neuron perspective by clustering neuron k ’s functional connectivity with neurons of

lower layers. This process involves two steps: (1) computing circuits, and (2) replacing a shared neuron with multiple virtual neurons for each circuit through clustering.

Step 1) Computing Circuits: To compute the edges of a circuit, we *explain* the activation of a neuron and attribute lower-level neurons. This naturally fits the idea of backpropagation-based feature attribution methods, specifically LRP [2]. LRP allows to efficiently backpropagate attribution scores through the network layer by layer, beginning at a latent neuron until the desired (input) layer is reached [2]. Concretely, the relevance R_j^l of an upper layer neuron j is generally distributed to lower-level neurons i as

$$R_{i \leftarrow j}^{l-1,l} = \frac{z_{i \rightarrow j}^{l-1,l}}{z_j^l} R_j^l \quad (1)$$

with $z_{i \rightarrow j}^{l-1,l}$ contributing to $z_j^l = \sum_i z_{i \rightarrow j}^{l-1,l}$ in the forward pass. Note that multiple refined ways to define $R_{i \leftarrow j}^{l-1,l}$ are proposed in literature for different layer types [16]. These relevance “messages” $R_{i \leftarrow j}^{l-1,l}$ refer to the *edges* of a circuit.

The circuit *nodes* are then characterized by node attributions computed via aggregation of the relevance messages:

$$R_i^{l-1} = \sum_j R_{i \leftarrow j}^{l-1,l}, \quad (2)$$

which reduces to $R_i^{L-1} = R_{i \leftarrow k}^{L-1,L}$ for the first backpropagation step when explaining neuron k in layer L as in Fig. 2.

For simplicity, we investigate in the following only nodes of the next lower-level layer $L - 1$. It is to note, that other methods besides LRP can be used for attributions here [10]. We therefore default to Gradient \times Activation as an efficient and universal attribution method implementing a simple LRP variant in ReLU-DNNs [26]. Thus, the circuit computation for neuron k in layer L simplifies for PURE to

$$R_i^{L-1} = A_i^{L-1} \frac{\partial A_k^L}{\partial A_i^{L-1}}, \quad (3)$$

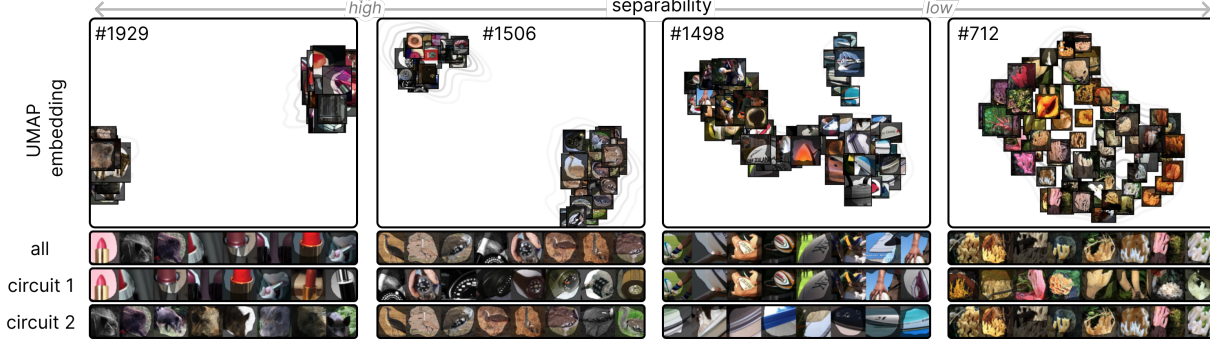


Figure 3. Applying PURE to neurons with varying degree of polysemanticity: We show UMAP embeddings with the maximally activating image patches, and the resulting reference sets before and after purification when identifying two circuits via k -means.

for circuit nodes i in lower-level layer $L - 1$, with activation A_k^L of neuron k in layer L , and partial derivative $\partial/\partial A_i^{L-1}$ w.r.t. lower-level layer activations A_i^{L-1} .

Step 2) Assigning Circuits: We represent a neuron by its most activating input samples. Then, for each of the top- n_{ref} activating input samples of a polysemantic neuron k in layer L , we compute the lower-level attributions R_j^{L-1} for all n neurons of layer $L - 1$ as given by Eq. (3) in a partial backward pass. If neuron j uses different circuits among the reference samples, we expect to see distinct clusters in the attribution vectors $\mathbf{R}^{L-1} \in \mathbb{R}^n$. To validate this assumption, we visualize a 2D UMAP [15] embedding of \mathbf{R}^{L-1} in Fig. 2. To find the distinct clusters, we use k -means clustering which results in centroids representing new virtual neurons for each circuit. For a new test sample, we can then identify the active circuit by computing \mathbf{R}^{L-1} and assigning it to the closest cluster centroid, *i.e.*, virtual neuron.

4. Experiments

We address the following research questions:

- (Q1) Can we find and purify polysemantic neurons?
- (Q2) How effective is PURE in disentangling representations compared to other approaches?

Experimental Setting We investigate the neurons in the penultimate layer of ResNet-34/50/101 models [12] pre-trained [29] on the ImageNet [25] dataset, and evaluate interpretability using the foundational models of CLIP [22] and DINOv2 [21]. We perform the analysis on the $n_{\text{ref}} = 100$ maximally activating input samples (based on max-pooling) for each neuron on the ImageNet test set. To generate feature visualizations, we crop samples such that only the important part of a neuron’s semantics remains [1], as illustrated in Fig. 2 (right) and detailed in Appendix A.1.

4.1. From Polysemanticity to Pure Features (Q1)

We begin with the quest to find polysemantic units by studying their feature visualizations, *i.e.*, their most activating

image patches. As a quantitative and objective measure for monosemanticity, we evaluate CLIP embeddings, where visually similar feature visualizations presumably result in small embedding distances [13, 30]. Concretely, for each neuron k we compute the distance matrix

$$\mathbf{D}_{ij}^k = \sqrt{(\mathbf{e}_i^{\text{CLIP}} - \mathbf{e}_j^{\text{CLIP}})^2} \quad (4)$$

between the CLIP embeddings $\mathbf{e}_i^{\text{CLIP}}$ of all pairs of feature visualizations (cropped reference samples) i and j .

To optimize the process of finding polysemantic units, we perform k -means clustering on the CLIP embeddings with a fixed number of two clusters. Then, inter- and intra-cluster distances ρ_k for neuron k are computed as

$$\rho_k^{\text{intra}} = \frac{\sum_{i,j \neq i}^{n_{\text{ref}}} \mathbf{D}_{ij}^k \mathbf{1}_{c_i=c_j}}{\sum_{i,j \neq i}^{n_{\text{ref}}} \mathbf{1}_{c_i=c_j}}, \quad \rho_k^{\text{inter}} = \frac{\sum_{i,j}^{n_{\text{ref}}} \mathbf{D}_{ij}^k \mathbf{1}_{c_i \neq c_j}}{\sum_{i,j}^{n_{\text{ref}}} \mathbf{1}_{c_i \neq c_j}} \quad (5)$$

with indicator function $\mathbf{1}_{c_i=c_j}$ equaling one if feature visualizations i and j have the same cluster index c , and zero else. A large difference $\rho_k^{\text{inter}} - \rho_k^{\text{intra}}$ indicates clearly separated clusters with different semantics.

In Fig. 3, neurons of varying degree of polysemanticity, as given by $\rho_k^{\text{inter}} - \rho_k^{\text{intra}}$, are shown for ResNet-50. Here, we also depict UMAP embeddings based on PURE attributions given by Eq. (3), and the feature visualizations before and after applying PURE. Note, that for PURE, we here disentangle one neuron into two virtual ones by clustering the lower-level attributions. As visible, polysemantic neurons such as #1929 and #1506 exist and can be effectively disentangled. The disentangled semantics can be visually different (“lipstick” and “boar”) or more related (“white spots” on dark circular objects or bird wings). On the other hand, we can also find rather monosemantic neurons, *e.g.*, #1498 and #712, that encode for lines and coral structure, respectively. More examples and more detailed results w.r.t. the distribution of polysemanticity are given in Appendix A.2.

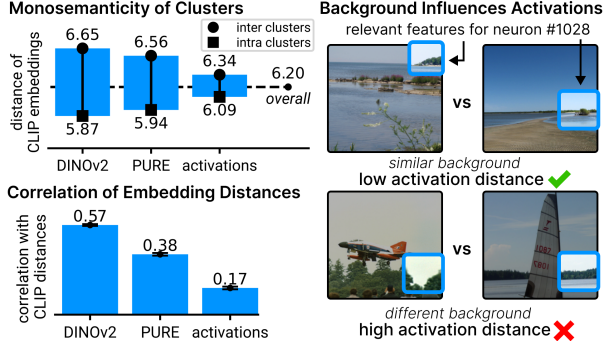


Figure 4. PURE leads to more interpretable representations as measured via CLIP embedding distances on feature visualizations (*top left*), thereby improving upon activation-based clustering and reaching almost DINOv2 scores. (*Bottom left*): Distances of CLIP embeddings between feature visualizations correlate with PURE embeddings significantly more than activations. (*Right*): Activations tend to overestimate distances when unrelated features vary.

4.2. Evaluating Feature Purification (Q2)

PURE aims to turn polysemantic neurons into purer virtual neurons that are easier to interpret, and works by computing and identifying the relevant circuits based on lower-level attributions R_i^{L-1} as by Eq. (3). Alternatively, O’Mahony *et al.* [20] propose activation-based disentanglement, where the activations A_i^L resulting from reference samples are clustered. When applied to a (polysemantic) neuron, both methods should result in more meaningful reference sample subsets for each disentangled feature, as, *e.g.*, in Fig. 3.

To systematically evaluate the interpretability of newly disentangled representations, we compute inter- and intra-cluster distances as defined in Eq. (5) using CLIP for the resulting sets of feature visualizations (cropped reference samples). Ideally, intra-cluster distances are low and inter-cluster distances are high, indicating well separated feature visualizations and more meaningful representations. The resulting CLIP embedding distances are reported in Fig. 4 (*top left*) for PURE and activation-based disentanglement for ResNet-101. As another baseline, we perform clustering on DINOv2 embeddings for the cropped reference samples. Here, DINOv2 represents an ideal visual separation, which is, however, computationally expensive as it requires both the computation of the cropped reference samples and a DINOv2 forward pass. The results show, that PURE leads to more disentangled representations than activation-based clustering, and is performance-wise close to DINOv2. Note that so far, clusters are computed using k -means with $k = 2$, but the same trends hold for different $k \in \{3, 4, 5\}$ and other ResNet architectures, as discussed in Appendix A.4.

In a second experiment, we dive deeper into why PURE attributions are more meaningful than latent activations. We thus investigate whether when two feature visualizations are

similar according to CLIP, they are also similar according to PURE attributions or activations. Concretely, for feature visualization pairs, we compute CLIP embedding distances via Eq. (4) and distances between PURE attributions as well as activations, and finally measure the correlation between the resulting distances of different methods. Please note, again, CLIP (and DINOv2) embeddings refer to the *cropped* reference samples, whereas PURE and activations are computed on the *full* reference samples. As shown in Fig. 4 (*bottom left*), PURE has higher alignment to CLIP compared to activations. We observe that activations lead to deviating distance scores in some cases, especially when the relevant semantics are very localized in reference samples, as shown in Fig. 4 (*right*) for neuron #1028 encoding for “vegetation on horizon”. Notably, activations take into account *all* present features in the *full* reference sample, which influences distances when unrelated features (*e.g.*, airplanes or boats) vary between samples. Whereas, conditional attributions as used by PURE are more specific to the actual task of a neuron. Correlation results for the other ResNet architectures and more examples when PURE or activation-based clustering diverges from CLIP are given in Appendix A.4.

5. Limitations and Future Work

So far, we assumed that embeddings of foundational models can be seen as ideal indicators for human interpretability and disentanglement. In future work, evaluation in controlled settings or using human feedback will be valuable.

Regarding PURE, a large ablation study will be interesting, *e.g.*, for clustering on full circuits (instead of only lower-level layer attributions), and using different feature attribution methods or other clustering approaches than k -means. Notably, PURE requires a partial backward pass to disentangle a neuron, which is computationally slightly more demanding than activation-based disentanglement.

It will be interesting to further study the advantages of purified units for XAI tools such as concept-based explanations, concept discovery and probing, or model correction.

6. Conclusion

We introduce PURE, a novel method for turning polysemantic neurons into multiple purer “virtual” neurons by identifying the active characteristic circuit of each pure feature. The purification of latent units allows to better understand latent representations, which is especially interesting for the growing and promising field of concept-based XAI. Using foundational models for evaluation, PURE results in significantly more purified features than activation-based approaches, which are less neuron-specific. We believe that our work will raise interest in investigating the benefits of cleaner representations for, *e.g.*, concept discovery, concept probing or model correction.

Acknowledgements

This work was supported by the Federal Ministry of Education and Research (BMBF) as grant BIFOLD (01IS18025A, 01IS180371I); the German Research Foundation (DFG) as research unit DeSBI (KI-FOR 5363); the European Union’s Horizon Europe research and innovation programme (EU Horizon Europe) as grant TEMA (101093003); the European Union’s Horizon 2020 research and innovation programme (EU Horizon 2020) as grant iToBoS (965221); and the state of Berlin within the innovation support programme ProFIT (IBB) as grant BerDiBa (10174498).

References

- [1] Reduan Achtabat, Maximilian Dreyer, Ilona Eisenbraun, Sebastian Bosse, Thomas Wiegand, Wojciech Samek, and Sebastian Lapuschkin. From attribution maps to human-understandable explanations through concept relevance propagation. *Nature Machine Intelligence*, 5(9):1006–1019, 2023. 1, 2, 3, 7
- [2] Sebastian Bach, Alexander Binder, Grégoire Montavon, Frederick Klauschen, Klaus-Robert Müller, and Wojciech Samek. On pixel-wise explanations for non-linear classifier decisions by layer-wise relevance propagation. *PloS one*, 10(7):e0130140, 2015. 2, 7
- [3] David Bau, Bolei Zhou, Aditya Khosla, Aude Oliva, and Antonio Torralba. Network dissection: Quantifying interpretability of deep visual representations. In *Proceedings of the IEEE conference on computer vision and pattern recognition*, pages 6541–6549, 2017. 1, 2
- [4] Kirill Bykov, Mayukh Deb, Dennis Grinwald, Klaus Robert Muller, and Marina MC Höhne. DORA: Exploring outlier representations in deep neural networks. In *ICLR 2023 Workshop on Pitfalls of limited data and computation for Trustworthy ML*, 2023. 1
- [5] Kirill Bykov, Laura Kopf, Shinichi Nakajima, Marius Kloft, and Marina Höhne. Labeling neural representations with inverse recognition. *Advances in Neural Information Processing Systems*, 36, 2024. 2
- [6] Nick Cammarata, Shan Carter, Gabriel Goh, Chris Olah, Michael Petrov, Ludwig Schubert, Chelsea Voss, Ben Egan, and Swee Kiat Lim. Thread: Circuits. *Distill*, 2020. <https://distill.pub/2020/circuits>. 2
- [7] Arthur Conmy, Augustine Mavor-Parker, Aengus Lynch, Stefan Heimersheim, and Adrià Garriga-Alonso. Towards automated circuit discovery for mechanistic interpretability. *Advances in Neural Information Processing Systems*, 36, 2024. 2
- [8] Maximilian Dreyer, Reduan Achtabat, Wojciech Samek, and Sebastian Lapuschkin. Understanding the (extra-)ordinary: Validating deep model decisions with prototypical concept-based explanations. *arXiv preprint arXiv:2311.16681*, 2023. 1
- [9] Nelson Elhage, Neel Nanda, Catherine Olsson, Tom Henighan, Nicholas Joseph, Ben Mann, Amanda Askell, Yuntao Bai, Anna Chen, Tom Conerly, Nova Das-Sarma, Dawn Drain, Deep Ganguli, Zac Hatfield-Dodds, Danny Hernandez, Andy Jones, Jackson Kernion, Liane Lovitt, Kamal Ndousse, Dario Amodei, Tom Brown, Jack Clark, Jared Kaplan, Sam McCandlish, and Chris Olah. A mathematical framework for transformer circuits. *Transformer Circuits Thread*, 2021. <https://transformer-circuits.pub/2021/framework/index.html>. 1, 2
- [10] Thomas Fel, Victor Boutin, Louis Béthune, Rémi Cadène, Mazda Moayeri, Léo Andéol, Mathieu Chalvidal, and Thomas Serre. A holistic approach to unifying automatic concept extraction and concept importance estimation. *Advances in Neural Information Processing Systems*, 36, 2024. 2
- [11] Michael Hanna, Ollie Liu, and Alexandre Variengien. How does gpt-2 compute greater-than?: Interpreting mathematical abilities in a pre-trained language model. *Advances in Neural Information Processing Systems*, 36, 2024. 1, 2
- [12] Kaiming He, Xiangyu Zhang, Shaoqing Ren, and Jian Sun. Deep residual learning for image recognition. In *Proceedings of the IEEE conference on computer vision and pattern recognition*, pages 770–778, 2016. 1, 3, 7
- [13] Neha Kalibhat, Shweta Bhardwaj, Bayan Bruss, Hamed Firooz, Maziar Sanjabi, and Soheil Feizi. Identifying interpretable subspaces in image representations. In *Proceedings of the 40th International Conference on Machine Learning*. JMLR.org, 2023. 3
- [14] Been Kim, Martin Wattenberg, Justin Gilmer, Carrie Cai, James Wexler, Fernanda Viegas, et al. Interpretability beyond feature attribution: Quantitative testing with concept activation vectors (tcav). In *International conference on machine learning*, pages 2668–2677. PMLR, 2018. 2
- [15] Leland McInnes, John Healy, Nathaniel Saul, and Lukas Großberger. Umap: Uniform manifold approximation and projection. *Journal of Open Source Software*, 3(29), 2018. 3, 8
- [16] Grégoire Montavon, Alexander Binder, Sebastian Lapuschkin, Wojciech Samek, and Klaus-Robert Müller. Layer-wise relevance propagation: an overview. *Explainable AI: interpreting, explaining and visualizing deep learning*, pages 193–209, 2019. 2
- [17] Anh Nguyen, Jason Yosinski, and Jeff Clune. Multifaceted feature visualization: Uncovering the different types of features learned by each neuron in deep neural networks. *arXiv preprint arXiv:1602.03616*, 2016. 2
- [18] Chris Olah, Alexander Mordvintsev, and Ludwig Schubert. Feature visualization. *Distill*, 2(11):e7, 2017. 1, 7
- [19] Chris Olah, Nick Cammarata, Ludwig Schubert, Gabriel Goh, Michael Petrov, and Shan Carter. Zoom in: An introduction to circuits. *Distill*, 5(3):e00024–001, 2020. 1, 2
- [20] Laura O’Mahony, Vincent Andrearczyk, Henning Müller, and Mara Graziani. Disentangling neuron representations with concept vectors. In *Proceedings of the IEEE/CVF Conference on Computer Vision and Pattern Recognition (CVPR) Workshops*, pages 3770–3775, 2023. 2, 4, 12
- [21] Maxime Oquab, Timothée Darcet, Théo Moutakanni, Huy Vo, Marc Szafraniec, Vasil Khalidov, Pierre Fernandez, Daniel Haziza, Francisco Massa, Alaaeldin El-Nouby, et al. Dinov2: Learning robust visual features without supervision. *arXiv preprint arXiv:2304.07193*, 2023. 3, 7

- [22] Alec Radford, Jong Wook Kim, Chris Hallacy, Aditya Ramesh, Gabriel Goh, Sandhini Agarwal, Girish Sastry, Amanda Askell, Pamela Mishkin, Jack Clark, et al. Learning transferable visual models from natural language supervision. In *International conference on machine learning*, pages 8748–8763. PMLR, 2021. 3, 7
- [23] Achyuta Rajaram, Neil Chowdhury, Antonio Torralba, Jacob Andreas, and Sarah Schwettmann. Automatic discovery of visual circuits. In *NeurIPS Workshop on Attributing Model Behavior at Scale*, 2023. 2
- [24] Tilman Raukur, An Chang Ho, Stephen Casper, and Dylan Hadfield-Menell. Toward transparent ai: A survey on interpreting the inner structures of deep neural networks. *2023 IEEE Conference on Secure and Trustworthy Machine Learning (SaTML)*, pages 464–483, 2022. 2
- [25] Olga Russakovsky, Jia Deng, Hao Su, Jonathan Krause, Sanjeev Satheesh, Sean Ma, Zhiheng Huang, Andrej Karpathy, Aditya Khosla, Michael Bernstein, et al. Imagenet large scale visual recognition challenge. *International journal of computer vision*, 115:211–252, 2015. 3
- [26] Avanti Shrikumar, Peyton Greenside, and Anshul Kundaje. Learning important features through propagating activation differences. In *International conference on machine learning*, pages 3145–3153. PMLR, 2017. 2
- [27] Johanna Vielhaben, Stefan Bluecher, and Nils Strodthoff. Multi-dimensional concept discovery (mcd): A unifying framework with completeness guarantees. *Transactions on Machine Learning Research*, 2023. 2
- [28] Kevin Ro Wang, Alexandre Variengien, Arthur Conmy, Buck Shlegeris, and Jacob Steinhardt. Interpretability in the wild: a circuit for indirect object identification in GPT-2 small. In *The Eleventh International Conference on Learning Representations*, 2023. 1, 2
- [29] Ross Wightman, Hugo Touvron, and Herve Jegou. Resnet strikes back: An improved training procedure in timm. In *NeurIPS 2021 Workshop on ImageNet: Past, Present, and Future*, 2021. 3
- [30] R. Zhang, P. Isola, A. A. Efros, E. Shechtman, and O. Wang. The unreasonable effectiveness of deep features as a perceptual metric. In *2018 IEEE/CVF Conference on Computer Vision and Pattern Recognition (CVPR)*, pages 586–595, Los Alamitos, CA, USA, 2018. IEEE Computer Society. 3

A. Appendix

In the appendix, we provide additional results for the main manuscript. Concretely, we give details on how we compute feature visualizations in Appendix A.1. Secondly, in Appendix A.2, the distribution of polysemanticity throughout neurons of ResNet [12] models is shown in higher detail. Further, we provide additional examples of resulting disentangled representations when applying PURE in Appendix A.3. Lastly, Appendix A.4 provides more results for evaluating feature interpretability after purification of neurons.

A.1. Feature Visualizations

An important part in understanding neurons are feature visualizations that aim to communicate the underlying semantics or concept of a neuron. In literature, either real data samples, or synthetically generated samples are used for visualization purposes [18]. Throughout our experiments, we utilize reference samples from the original dataset to render visualizations that are as natural as possible, ideally staying in-distribution w.r.t. the foundational models of CLIP [22] and DINO [21] in evaluations.

When using reference samples from the dataset, it is crucial to crop images to the actually important part for a neuron, as semantics can be very localized, as, *e.g.*, visible in Fig. A.1 when comparing “full” against “cropped” samples. In order to detect this “relevant” part, Achtabat *et al.* [1] propose to explain neuron activations using LRP [2] in a first step, which results in neuron-specific input feature attributions. Specifically for convolutional layers, the maximum activation of a feature map is explained. In a second step, the attributions are smoothed using a Gaussian filter with kernel size K , normalized to a maximum value of one, and the image cropped and masked to include only attributions above a threshold of T . For the masked part, black color is overlaid with 40 % transparency.

When evaluating visualizations with CLIP and DINO, we use cropped samples with $K = 5$ and $T = 0.01$. We refrain from masking samples, as masks could introduce out-of-distribution data. For visualizations in plots, we include masks as proposed by [1] using $K = 51$ and $T = 0.01$.

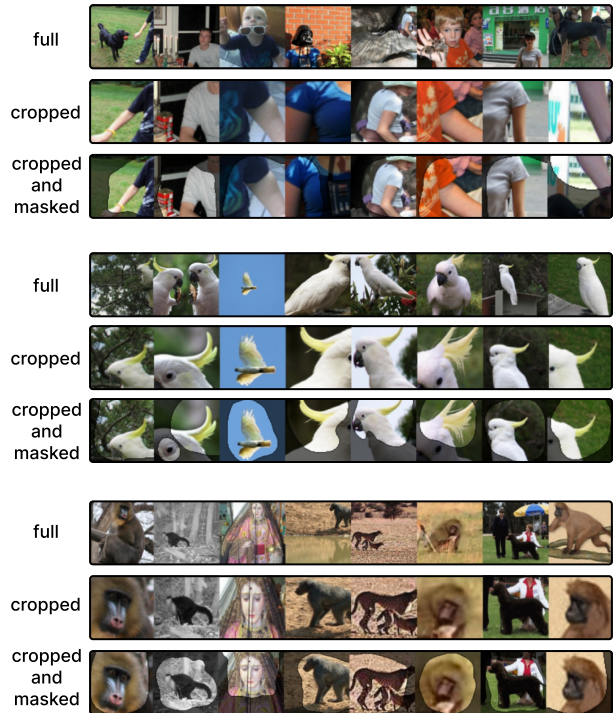


Figure A.1. Feature visualizations for neurons #1028 (*top*), #1029 (*middle*) and #1030 (*bottom*) for full, cropped-only and cropped as well as masked reference samples. It is visible that cropping improves visualizations by removing irrelevant and distracting image parts not relevant for a neuron semantics.

A.2. Distribution of Polysemanticity

In Sec. 4.1, we measure the degree of monosemanticity by using CLIP embeddings and computing distances in embedding space for feature visualization pairs of a neuron. Small distances between embeddings presumably correspond to visually similar feature visualizations.

For polysemantic neurons, where, *e.g.*, two monosemantic features superimpose, we would see two distinct clusters for each set of reference samples (of each pure feature) in a UMAP [15] embedding. The inter-cluster distance, in this case, will be high, whereas intra-cluster distance will be low. In the following, we apply k -means clustering ($k = 2$) on CLIP embeddings for all neurons w.r.t. the 100 most activating reference samples, and measure the overall as well as inter- and intra-cluster distances as given by Eq. (5).

In Fig. A.2, we show the distribution of distances (intra- and inter-cluster distance difference, and overall distance) for ResNet-50. It is apparent, that for most neurons, clustering improves the visual similarity of feature visualizations according to CLIP. However, for some (a few hundred of the 2048 neurons), a larger improvement can be seen, indicating more polysemantic neurons.

Examples with UMAP embeddings and clustered reference samples for neurons of varying degrees of polysemanticity are shown in Fig. A.2 (bottom). Neurons #1028 and #1984 have low overall CLIP embedding distance and correspond to monosemantic features, *e.g.*, “human arms” and “human crowds”, respectively. Further, neurons #696 and #107 have large improvement in embedding distance when clustered, indicating polysemanticity, *e.g.*, “dog face” vs. “text/horizontal lines” and “shark under water”, respectively. Lastly, we show neuron #1177 with high overall distances, where clustering does not strongly decrease distances. This is apparently due to three existing semantics in the neuron, where clustering using two clusters is not optimal for disentanglement.

Additionally, we provide distribution plots for ResNet-34 and ResNet-101 in Fig. A.3. It is to note, that ResNet-34 only consists of 512 instead of 2048 neurons in the penultimate layer. Comparing ResNet-34 and ResNet-100 distributions, improvements in CLIP embedding distances through clusters seem to be lower for ResNet-34, potentially indicating a smaller degree of polysemanticity. However, we leave comparison across architectures for future work.

A.3. Examples for Applying PURE

In the following, we present additional examples when applying PURE to neurons with different separability levels, which, for neurons with high separability score, leads to multiple virtual (ideally more disentangled) neurons.

As in Sec. 4.1, we create two virtual neurons using k -means for each neuron of a ResNet-50 in the penultimate layer. We then visualize the UMAP embeddings of the

PURE attributions given by Eq. (3) and the resulting clustered feature visualizations.

In Fig. A.4 we show five *randomly sampled* neurons which exhibit different levels of separability; we see that both monosemantic (#162 and #1804) and polysemantic (#141, #1657, and #310) neurons can be found. Regarding the polysemantic units #1657 and #310, PURE leads to well separated reference samples. For #141, three semantics seem to exist, where clustering with two clusters does not optimally disentangle the unit.

In Fig. A.5, we focus on neurons with higher degree of polysemanticity (indicated by a large inter-cluster distance and low intra-cluster distance on PURE embeddings), which can be meaningfully disentangled into multiple virtual monosemantic neurons using PURE. For instance, *e.g.* neuron #1381 encodes both for “printed letters” and “orca”, which PURE effectively disentangled. Similarly, neurons #916 and #915 refers to semantics such as “two dogs” and “bird wings” and of “badger” and “ketchup and mustard in hot dog” features, respectively.

Fig. A.6 illustrates examples of neurons encoding for pure features with small differences in inter- and intra-cluster distances (with a low level of separability). Noteworthy, instances include neurons such as #1, which represents “chain”, or neuron #160, encoding “seashore/shore”.

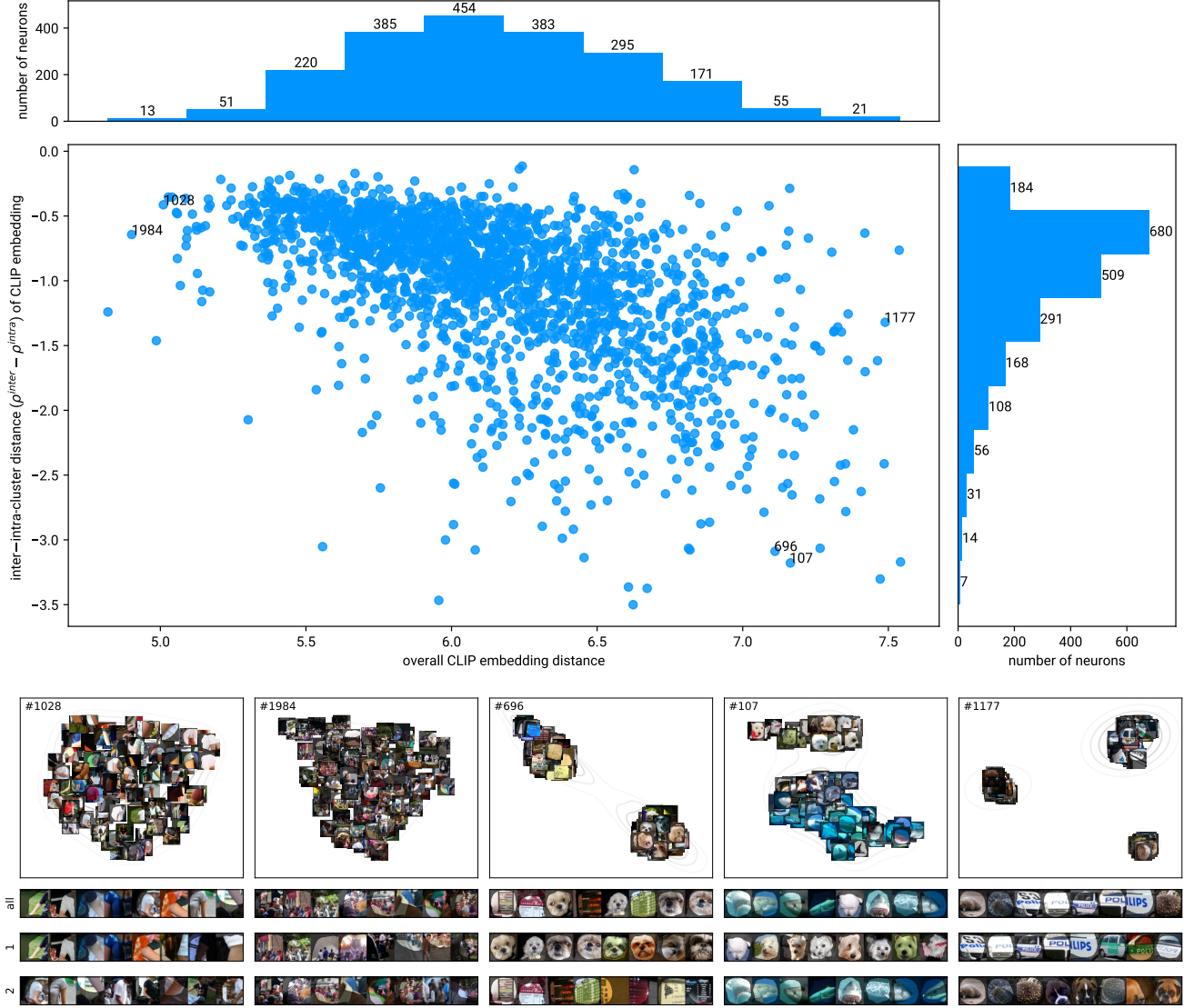


Figure A.2. Distribution of CLIP embeddings distances for all neurons of the ResNet-50 model. We show the overall distances between feature visualizations of a neuron on the horizontal axis, and the difference between inter- and intra-cluster distance after clustering visualizations into two clusters on the vertical axis. (*Bottom*): Examples are given for neurons with various degrees of polysemanticity. UMAP embeddings for PURE attributions as well as reference samples for the original and two virtual neurons are shown when applying PURE.

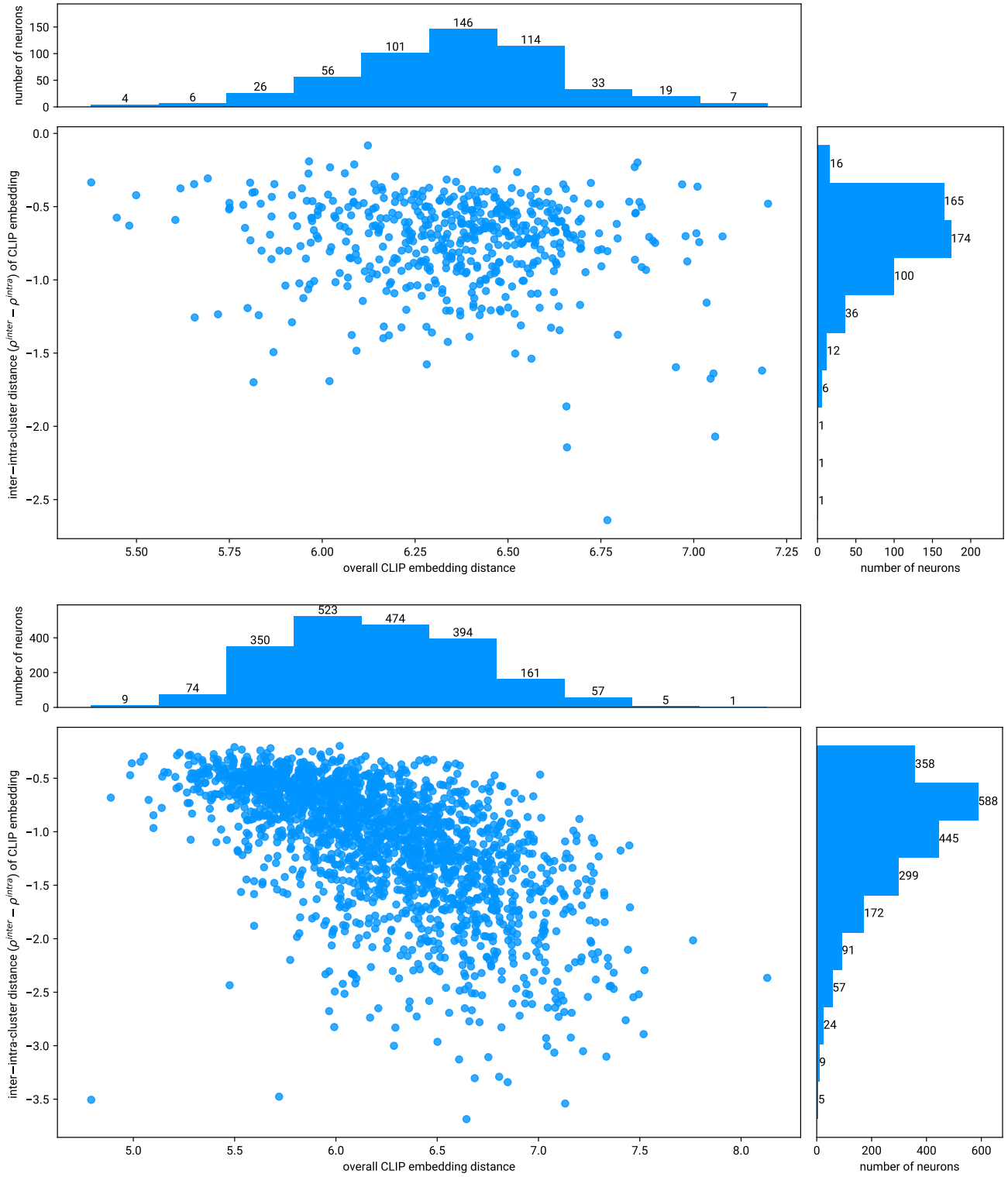


Figure A.3. Distribution of CLIP embeddings distances for all neurons of the ResNet-34 (*top*) and ResNet-101 (*bottom*) model. We show the overall distances between feature visualizations of a neuron on the horizontal axis, and the difference between inter- and intra-cluster distance after clustering visualizations into two clusters on the vertical axis.



Figure A.4. Examples of applying PURE to *randomly chosen* neurons. Here we see the UMAP embeddings of the maximally activating patches, and the resulting reference sets before and after applying purification when identifying two circuits via k -means. In ResNet-50 neurons with different level of polysemanticity can be found.



Figure A.5. Examples of applying PURE to neurons with *high degree of polysemanticity*. Here we see the UMAP embeddings of the maximally activating patches, and the resulting reference sets before and after applying purification when identifying two circuits via k -means. We show that neurons with high degree of polysemanticity can be successfully disentangled into two (or more) monosemantic neurons.

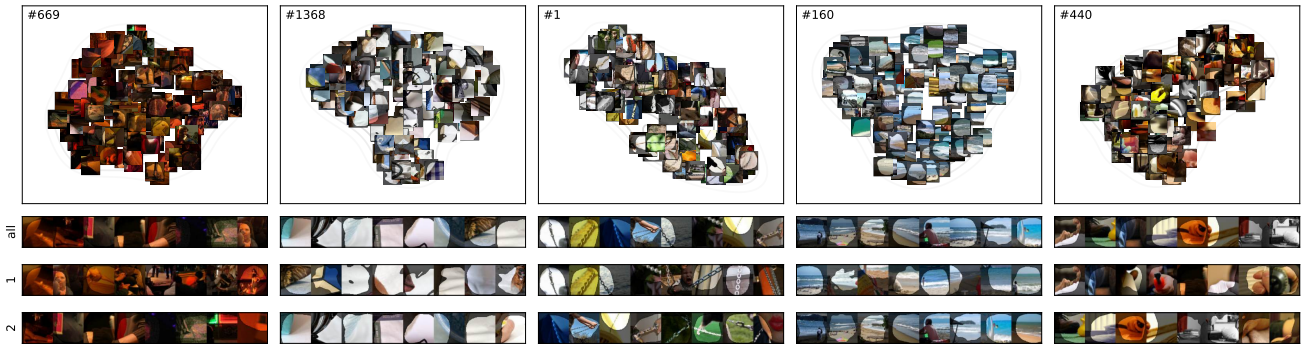


Figure A.6. Examples applying PURE to neurons with *low degree of polysemanticity*. Here we see the UMAP embeddings of the maximally activating patches, and the resulting reference sets before and after applying purification when identifying two circuits via k -means. The neurons encode one or similar features in this case, resulting in one circuit to be identified.

A.4. Evaluating Neuron Purification using CLIP

In Sec. 4.2, we evaluate the effectiveness of disentanglement via CLIP. Specifically, we create k new virtual neurons for each neuron by clustering the 100 most activating reference samples of a neuron into k clusters. Then, the reference samples of each cluster are evaluated using CLIP, where ideally, the CLIP embedding distance decreases inside clusters and increases across clusters, indicating well (visually) separated clusters. In Fig. A.8, we present additional results for the main manuscript (where $k = 2$ and ResNet-101 model results are shown) for ResNet-34 and ResNet-50 for $k \in \{2, 3, 4, 5\}$. For all experiments, PURE leads to better cluster separation than activation-based clustering. Notably, the higher k is, the lower intra-cluster distances are in general, indicating visually more monosemantic feature visualizations per virtual neuron. However, inter-cluster distance often decreases when k is increased, which indicates that most neurons are rather monosemantic, as also discussed in Appendix A.2.

A clustering that is aligned with CLIP results from similar distances between feature visualization pairs according to the respective methods. Concretely, CLIP and DINOv2 embeddings $\mathbf{e}_i^{\text{CLIP}}$ (and $\mathbf{e}_i^{\text{DINOv2}}$) are computed using feature visualizations (cropped reference samples) as the input for reference sample i w.r.t. to a neuron p in layer L . For PURE distances are computed on lower-level layer attributions \mathbf{R}^{L-1} as given by Eq. (3) when explaining neuron p . Further, for activation-based distances, activations \mathbf{A}^L in layer L are used, as proposed by [20]. The more aligned to CLIP, the higher the correlation of distances between the methods is. We provide additional results for Sec. 4.2 with results for ResNet-50 and ResNet-34 in Fig. A.7, for which PURE also shows higher correlations than activation. The correlation analysis involves examining the pairwise distances for the top-50 most activating reference samples across all neurons in the penultimate layer. The standard error of mean is computed by partitioning distances in 30 subsets (over which the mean is computed).

A.4.1 When Disentanglement Diverges from CLIP

In the following, we present examples, when activation-based or PURE attribution-based clustering of reference samples diverges from how CLIP embeddings cluster feature visualizations for the ResNet-50.

Activation We observe unfaithful clustering with activations when a significant portion of feature visualizations is of a single class, leading to high activation similarities (due to similar features present in the reference samples). The reference samples of the same class dominate in clustering, leading to all samples from different classes being clustered in another cluster. This is given, e.g., for neurons #143

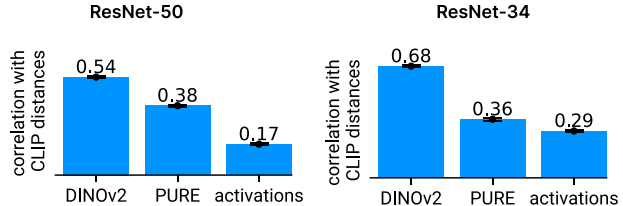


Figure A.7. Correlation between feature visualization distances of CLIP to other methods for ResNet-50 (left) and ResNet-34 (right), which extends the results given in Fig. 4.

(class “custard apple”), #385 (class “shoji”), #614 (class “lacewing”), or #1055 (class “buckeye”). Further, all reference samples can have small activation similarity if, e.g., most are from different classes, which is the case for neuron #1147, leading to noisy clustering.

PURE Similarly, as for activation, attributions can result in different clustering (compared to CLIP), e.g., for neurons #614 or #1055 as shown in Fig. A.10, where very small distances between reference samples from the same class (“lacewing” and “buckeye”, respectively) lead to unaligned clustering. For other neurons, semantics can be more abstract and difficult to understand, such as #1032 (radially outspreading lines) or #1121. In these cases, CLIP seems to result in clustering reference samples corresponding to same depicted object classes (e.g., dogs or monkeys, respectively). This is also the case for neuron #271, where the semantics seems to correspond to triangular shapes that can be found for toy windmills or dog ears. Here, CLIP separates dogs from windmills, even though they correspond to the same semantics, indicating also a disadvantage of using CLIP for evaluation. Especially for abstract concepts, attributions can result in low distances, whereas according to CLIP, bigger distances exist. This also raises the question whether the ultimate goal of disentanglement is to separate clusters according to *visual* difference or *semantic* difference (as seen by the model).

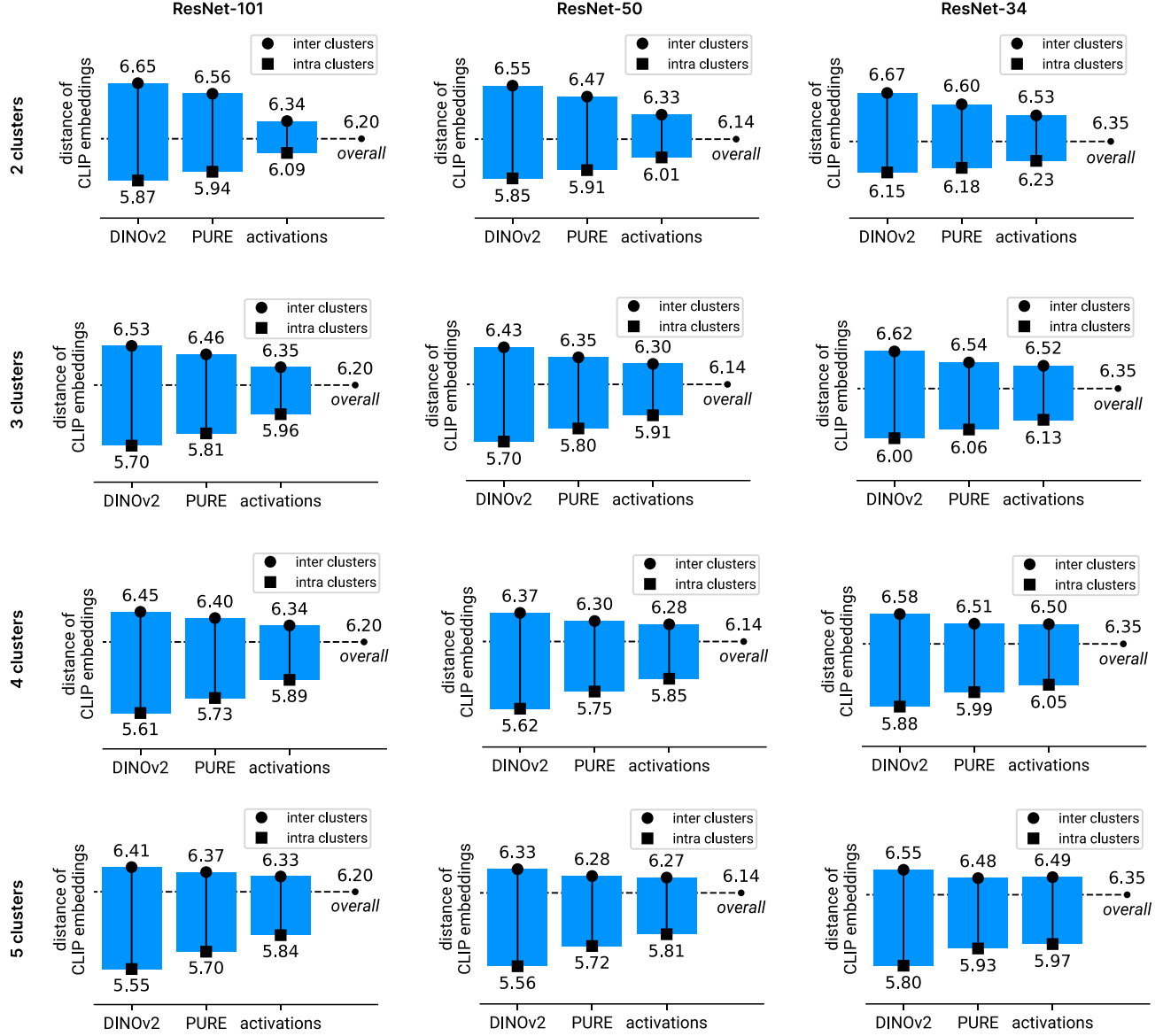


Figure A.8. Results for measuring the degree of monosemanticity of clustered feature visualizations using CLIP embedding distances, as discussed in Sec. 4.2 for all ResNet architectures and different number of clusters (virtual neurons).



Figure A.9. Examples for diverging disentanglement using activations compared to CLIP embeddings for the ResNet-50 model. We show UMAP embeddings and the corresponding feature visualizations before (“all”) and after (cluster “1” and “2”) disentanglement using activations (*top*) and CLIP embeddings (*bottom*)



Figure A.10. Examples for diverging disentanglement using PURE attributions compared to CLIP embeddings for the ResNet-50 model. We show UMAP embeddings and the corresponding feature visualizations before (“all”) and after (cluster “1” and “2”) disentanglement using attributions (*top*) and CLIP embeddings (*bottom*)